1-1-2019

Role of Charge Density Wave in Monatomic Assembly in Transition Metal Dichalcogenides

Haifeng Feng
University of Wollongong, haifeng@uow.edu.au

Zhongfei Xu
Beihang University, xuzfei@buaa.edu.cn

Jincheng Zhuang
Beihang University, jincheng@uow.edu.au

Li Wang
University of Wollongong, lw037@uowmail.edu.au

Yani Liu
University of Wollongong, yl100@uowmail.edu.au

See next page for additional authors

Role of Charge Density Wave in Monatomic Assembly in Transition Metal Dichalcogenides

Abstract

The charge density wave (CDW) in transition metal dichalcogenides (TMDs) has drawn tremendous interest due to its potential for tailoring their surface electronic and chemical properties. Due to technical challenges, however, how the CDW could modulate the chemical behavior of TMDs is still not clear. Here, this work presents a study of applying the CDW of NbTe 2 , with a high transition temperature above room temperature, to generate the assembling adsorption of Sn adatoms on the surface. It is shown that highly ordered monatomic Sn adatoms with a quasi-1D structure can be obtained under regulation by the single-axis CDW of the substrate. In addition, the CDW modulated superlattices could in turn change the surface electronic properties from semimetallic to metallic. These results demonstrate an effective approach for tuning the surface chemical properties of TMDs by their CDWs, which could be applied in exploring them for various practical applications, such as heterogeneous catalysis, epitaxial growth of low-dimensional materials, and future nanoelectronics.

Disciplines

Engineering | Physical Sciences and Mathematics

Publication Details

Feng, H., Xu, Z., Zhuang, J., Wang, L., Liu, Y., Xu, X., Song, L., Hao, W. & Du, Y. (2019). Role of Charge Density Wave in Monatomic Assembly in Transition Metal Dichalcogenides. Advanced Functional Materials, 29 (15), 1900367-1-1900367-7.

Authors

Haifeng Feng, Zhongfei Xu, Jincheng Zhuang, Li Wang, Yani Liu, Xun Xu, Li Song, Weichang Hao, and Yi Du

Role of charge density wave in monatomic assembly in transition metal dichalcogenides

Haifeng Feng, Zhongfei Xu, Jincheng Zhuang, Li Wang, Yani Liu, Xun Xu, Li Song, Weichang Hao, and Yi Du**

Dr. H. Feng, Dr. L. Wang, Y. Liu, Dr. X. Xu, Dr. Y. Du,
Institute for Superconducting and Electronic Materials (ISEM), Australian Institute for Innovative Materials (AIIM), University of Wollongong, Wollongong, NSW 2500, Australia
E-mail: yi_du@uow.edu.au (Y.D.) and xun@uow.edu.au (X. X.)

Dr. Z. Xu, A/Prof. J. Zhuang, Y. Liu, Dr. X. Xu, Prof. W. Hao, Dr. Y. Du
School of Physics and BUAA-UOW Joint Research Centre, Beihang University, Beijing 100191, P. R. China

Prof. L. Song
National Synchrotron Radiation Laboratory, CAS Center for Excellence in Nanoscience, University of Science and Technology of China, Hefei 230029, P. R. China

Keywords: transition metal dichalcogenides, charge density wave, surface chemical adsorption, scanning tunneling microscopy, monatomic assembly

Abstract

The charge density wave (CDW) in transition metal dichalcogenides (TMDs) has drawn tremendous interest due to its potential for tailoring their surface electronic and chemical properties. Due to technical challenges, however, how the CDW could modulate the chemical behavior of TMDs is still not clear. Here, this work presents a study of applying the CDW of $NbTe_2$, with a high transition temperature above room temperature, to generate the assembling adsorption of Sn adatoms on the surface. It is shown that highly ordered monatomic Sn adatoms with a quasi-one-dimensional structure can be obtained under regulation by the single-axis CDW of the substrate. In addition, the CDW modulated superlattices could in turn change the surface electronic properties from semi-metallic to metallic. These results demonstrate an effective approach for tuning the surface chemical properties of TMDs by their CDWs, which could be applied in exploring them for various practical applications, such as heterogeneous catalysis, epitaxial growth of low-dimensional materials, and future nanoelectronics.

Main Text

Transition metal dichalcogenides (TMDs), are layered materials consisting of repeating chalcogen-metal-chalcogen layers, with strong in-plane covalent bonding but weak interaction through out-of-plane van der Waals (vdW) forces.[1-4] Rich electronic phases, including metallic, semiconducting, superconducting, charge density wave (CDW), and topological, make TMDs appealing as multifunctional materials, which are diverse in terms of their polytypes and dimensionalities, as well as the variation in their transition metals and chalcogens.[5-11] A CDW emerges when the temperature is lower than a transition temperature T_c, in which instability of the electronic states close to the Fermi level, E_F, leads to a modulation of the electronic charges and lattice. Abundant phases have been found in TMDs, for instances, a number of MX_2 phases (where M = Ti, Nb and Ta; X = S, Se, and Te). Several different mechanisms, including Fermi surface (FS) nesting,[8,12] saddle-point singularities,[13,14] and electron-phonon coupling (EPC),[15-18] have been proposed regarding the origin of CDWs in TMDs. The CDW has received intense interest because it provides a platform for interpreting unconventional superconductivity and strongly correlated electron systems.[19-22] Additionally, other newly discovered phenomena, for example, semiconductor-metal transitions in TMDs triggered by a CDW phase transition, offer very promising pathways for developing future electronic devices.[23-30] These studies implied that CDWs in TMDs possess the alluring ability to determine or modulate their electronic properties. Recently, CDWs in TMDs were found to play a vital role in versatile applications besides electronics, such as catalysis and energy storage.[31-33] In particular, for heterogeneous catalysis, CDWs are expected to be feasible for tailoring the adsorption scheme of reactants and active sites via tuning the surface electronic properties of catalysts.[34-37] Due to technical challenges, however, it remains unclear how the CDW modulates the chemical behavior by tuning the surface electronic properties in TMDs.

Here, we utilized the CDW of $NbTe_2$, which has a high transition temperature above room temperature,[38,39] to modulate the monatomic assembly behavior of Sn on the surface. Characterization by scanning tunneling microscopy (STM) showed that monatomic Sn adatoms are regulated by the single-axis CDW of the substrate, forming a quasi-one-dimensional (1D) structure with indirect repulsive interaction. With increasing coverage, highly ordered commensurate Sn patterns with equal space prevail on the surface. In addition, through investigations by scanning tunneling spectroscopy (STS) and density functional theory (DFT) calculations, it was found that the CDW modulated superlattices could, in turn, change the surface electronic properties from semi-metallic to metallic. The direct observation of a CDW regulated ordered superlattice on the TMD surface demonstrates an effective approach for tuning the surface chemical properties, which will promote their exploration in various practical applications, such as heterogeneous catalysis, epitaxial growth of low-dimensional materials, and future nanoelectronics.[40-43]

We first characterized the surface structure and CDW phases of an in-situ cleaved $NbTe_2$ substrate by STM. **Figure 1a** illustrates layered $NbTe_2$ in the monoclinic crystal structure (distorted octahedral). Adjacent layers are weakly stacked to form the bulk crystal. Each single layer is composed of a Nb layer sandwiched by two Te layers, forming a Te-Nb-Te structure. Due to the formation of the CDW, the displacement of Nb atoms from the centers of the octahedra leads to a periodic lattice distortion (PLD) with a 3 × 1 CDW supercell (red parallelogram), as illustrated in Figure 1a. Figure 1b shows a large-scale STM image of the cleaved surface with large flat terraces and several small residual islands. Figure 1c presents a high-resolution STM image that clearly shows the stripe-like structures on surface, with the 3 × 1 CDW unit cell marked by the red parallelogram (See the height profile in Figure S1 in Supporting Information). The bright features and defects on the stripes can be assigned to top surface Te atoms and Te vacancies, respectively.[31] The fast Fourier transform (FFT) of the STM image in Figure 1d further confirms the coexistence of 3 × 1 supercells (red circles) with

the Te atomic lattice (white circles), with an angular deviation (around 6°) from the regular rectangle, agreeing well with the distorted octahedral structure.

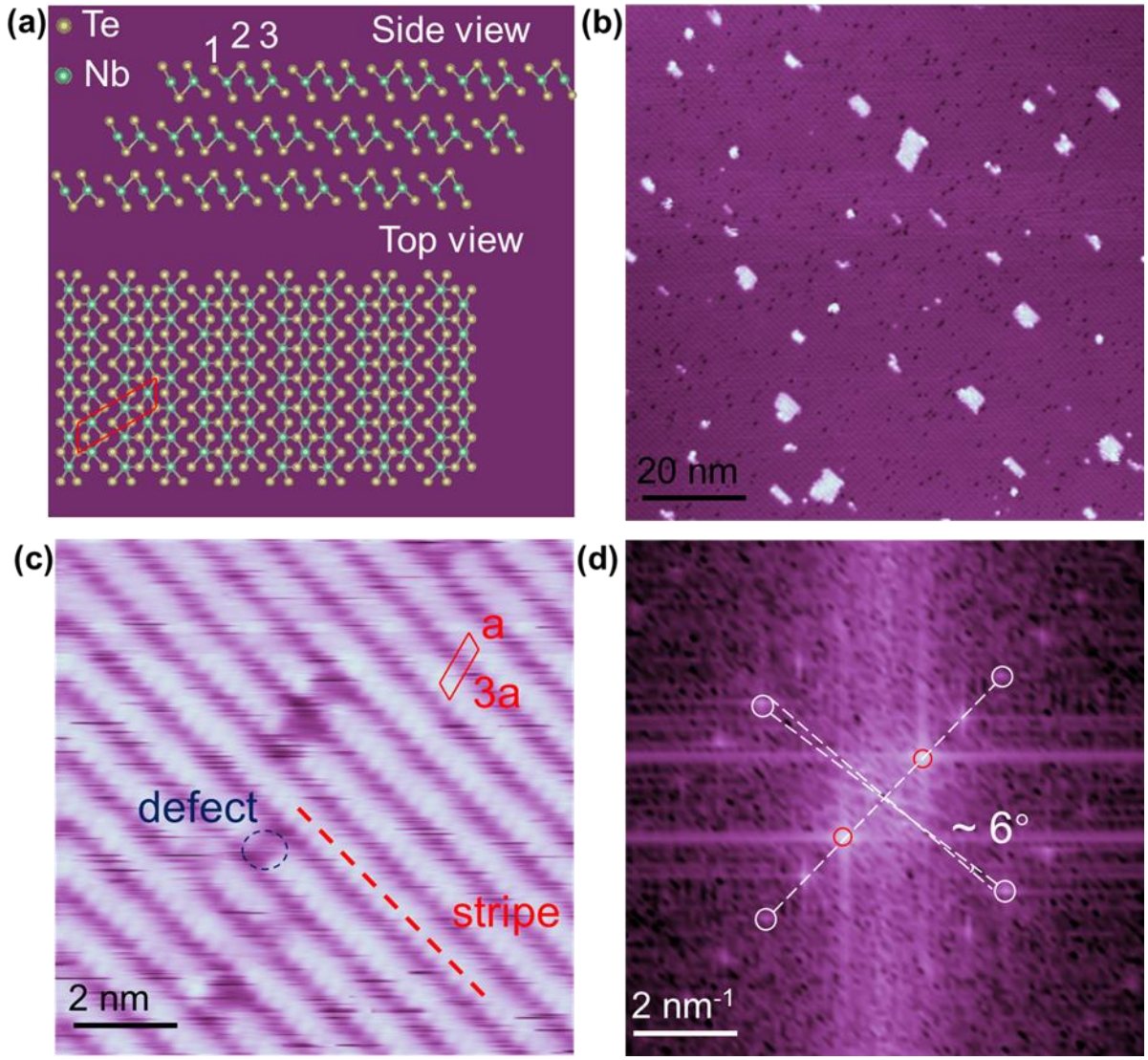

Figure 1. (a) Schematic diagram of the crystal structure of $NbTe_2$ in the monoclinic structure from both the side view and the top view. The unit cell of the 3 × 1 CDW is indicated by the red parallelogram. (b) STM image of the large-scale surface of the in-situ cleaved $NbTe_2$ single crystal (-1.5 V, 50 pA). (c) High-resolution STM image of the $NbTe_2$ surface, with a stripe indicated by the red dashed line and a surface Te vacancy indicated by the blue dash circle (50 mV, 50 pA). (d) The fast Fourier transform (FFT) of the STM image in c. The white circles indicate the first-order Bragg peaks. The red circles indicate the stripe peaks. The angle of around 6° indicates the lattice distortion between the crystallographic axes on the surface (between a stripe and its perpendicular direction).

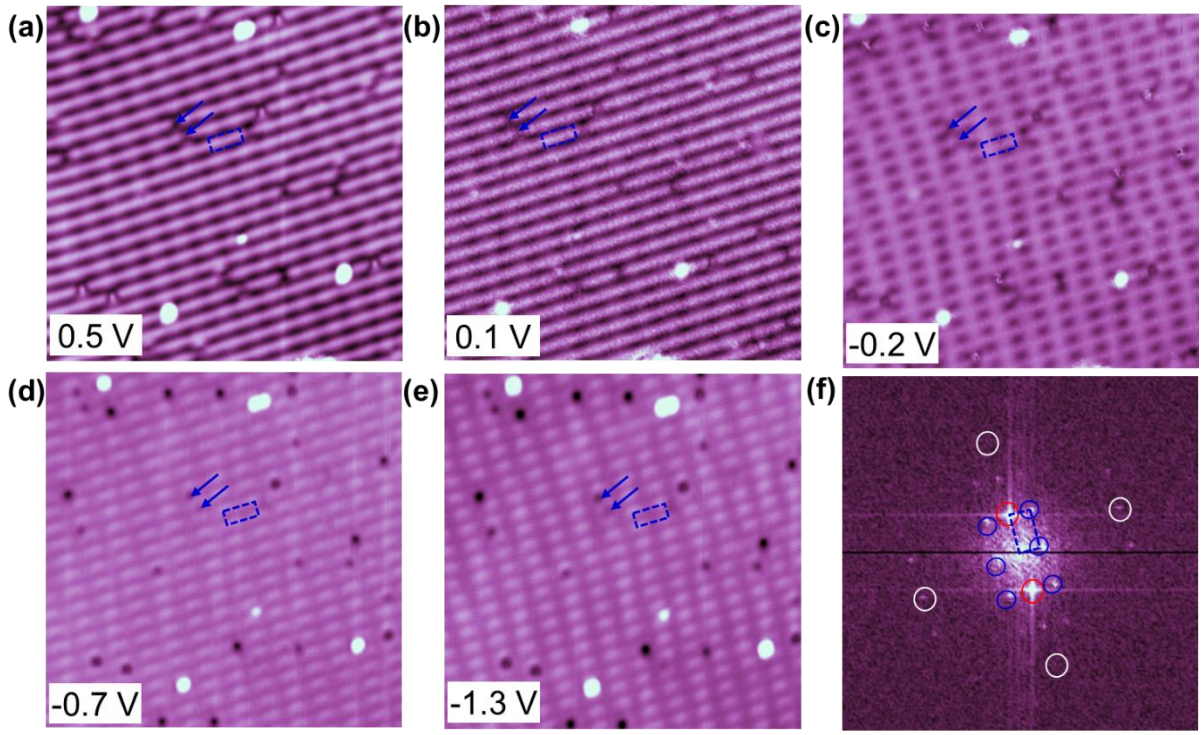

Figure 2. (a-e) Bias dependent STM image of $NbTe_2$ surface, in the range from -1.3 V to 0.5 V. All images were obtained at approximately the same surface location with a constant current of 300 pA. The unit cell of an additional CDW order is marked by the blue rectangle, with two characteristic defects marked as spatial reference points. The size of the images is 20 nm × 20 nm. (f) FFT pattern of the STM image in a. The white circles indicate the first-order Bragg peaks. The red circles indicate the stripe peaks. The blue circles and the rectangle indicate the peak and the unit cell of the additional CDW order, respectively.

The stripe structure induced by CDW was also examined by bias dependent imaging. An additional superstructure was surprisingly observed, as shown in **Figure 2a-e**. In the bias range between 0.1 V and 0.5 V, the 3 × 1 CDW induced stripe morphology was clearly observed, with an additional superstructure starting to appear on the surface. Whereas, when the bias was lowered to -0.2 V, as shown in Figure 2c, the additional superstructure, with the unit cell marked by the blue rectangle, instead became the clearer one on the surface. With further decrease of the sample bias, this superstructure dictated the morphology in the STM images. Specifically, the position of the superstructure with reference to the stripes varied from the hill to the valley of the stripes, as indicated by the two blue arrows at Te vacancies as spatial reference points. The bias dependent intensity and position suggest that the additional superstructure can be regarded as an electronic state.

By carefully measuring the lattice along the stripe and analyzing the FFT of the STM image in Figure 2f, the unit cell was found to be very close to $\sqrt{19} \times 3\sqrt{3}/2$. This superstructure has been assigned to an incommensurate CDW phase of $\sqrt{19} \times \sqrt{19}$ at low temperature (compared with 1 ×3 CDW) in previous studies, through experiments involving electron diffraction and neutron diffraction.[44,45] The $\sqrt{19} \times \sqrt{19}$ CDW phase was reported to be a triple-axis periodic structure, however, rather than the single-axis structure observed in Figure 2. This difference can be explained by the existence of domains separated by boundaries with an angle of either 60° or 120° across the single crystal, as shown in Figure S2 in the Supporting Information. Therefore, two CDW phases, a commensurate 3 × 1 phase and an incommensurate $\sqrt{19} \times 3\sqrt{3}/2$ phase, are found to coexist on the surface of $NbTe_2$ at 78 K.

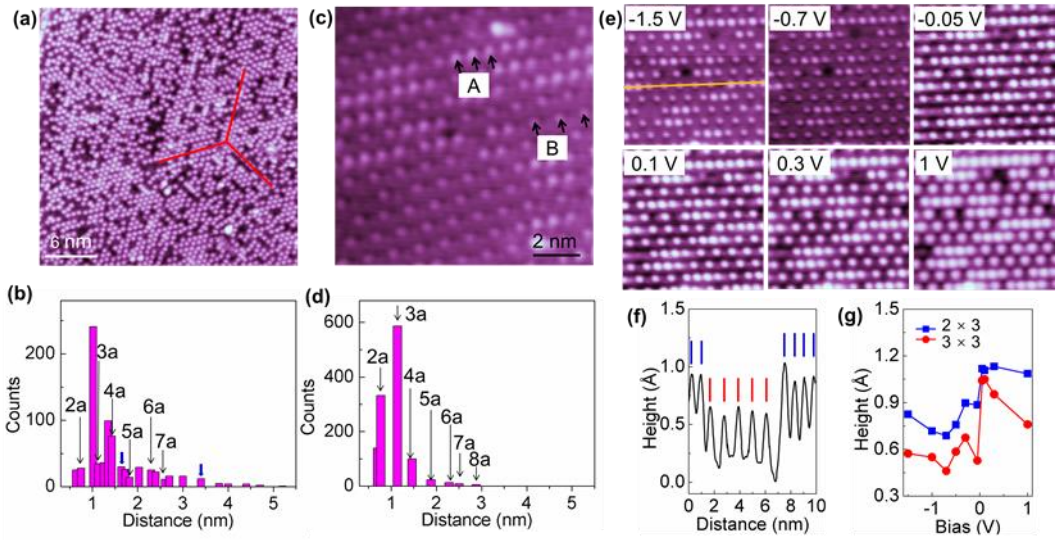

Figure 3. (a) STM image of the surface of $NbTe_2$ covered by 0.1 ML Sn atoms. The red lines indicate the orientations of domains of the $NbTe_2$ substrate (3 V, 50 pA). (b) Histogram of the nearest-neighbor pair-distances of Sn adatoms along the stripe direction of the substrate with coverage of 0.1 ML, which are commensurate to the lattice parameter *a* and $\sqrt{19}a$, as indicated by the black arrows and blue arrows, respectively. (c) STM image of the surface of $NbTe_2$ covered by 0.3 ML Sn atoms, showing two dominant ordered structures marked as A and B, respectively (-1.7 V, 50 pA). (d) Histogram of the nearest-neighbor pair-distance of Sn adatoms along the stripe direction of the substrate with coverage of 0.3 ML, with those commensurate to *a* indicated by the black arrows. (e) Bias dependent STM images of the $NbTe_2$ surface covered by 0.3 ML Sn adatoms (image size is 10 nm × 10 nm). All images were acquired at approximately the same surface location with a constant current of 300 pA. (f) Height profile of the line in e. (g) Variation of the heights of Sn adatoms in the 3 × 2 order and 3 × 3 order with the sample bias.

As discussed, the intrinsic periodic charge potential and lattice distortion observed for CDW phase could have a great impact on the surface electronic structure, and consequently, affect the surface chemical behavior towards reactant adsorption. To reveal the role of the CDW in the surface reactant adsorption, we carried out an in-situ deposition of Sn on the surface of $NbTe_2$ at room temperature. Sn is well-known as an excellent electrocatalyst both for reducing CO_2 and for modifying the catalytic activity and selectivity of other catalysts.[46-48] We first deposited around 0.1 monolayer (ML) of Sn atoms on the surface (1 ML is defined as the number of top Te atoms, ~ 8×10^{14} atoms cm^{-2}), which was then transferred to the STM chamber for characterization at 78 K. As shown in **Figure 3a**, the round and bright protrusions, identified as single Sn adatoms, have all arranged themselves along the 3 × 1 CDW induced stripe directions, as indicated by the red lines. This indicates that $NbTe_2$ was acting as a template in producing such a 1D structure, with its CDW providing an intrinsic 1D periodic charge potential. The 1D Sn adatoms along the stripes were then analyzed by measuring the nearest-neighbor (NN) pair distance of two adjacent Sn atoms, as shown in the histogram in Figure 3b. It was found that Sn adatoms did not arrange themselves randomly along the stripe, but preferentially assembled with several NN distances, either commensurately (indicated by the black arrows) or incommensurately. The minimum and maximum NN distances observed are 0.64 nm and 5.2 nm, respectively, indicating that an indirect long-range interaction along the stripe exists between Sn adatoms to produce such superstructures. Among them, the first two prevailing NN distances on the surface are neither the commensurate ones nor are they commensurate with $\sqrt{19}a$ but are 1.02 nm and 1.35 nm which are slightly smaller than $3a$ (1.13 nm) and $4a$ (1.43 nm), respectively.

Whereas, on increasing the coverage to 0.3 ML, the Sn adatoms exhibited a well-ordered commensurate arrangement along the stripe, as shown in Figure 3c and 3d, with the two major kinds of superlattices, type A (brighter protrusions than type B, in a solo order of 3 × 2) and type B (in a 3 × b order, with b ranging from $3a$ to $8a$), observed on the surface, according to

their brightness. This coverage dependent phenomenon suggests that the indirect interaction between Sn adatoms should be repulsive, which occurs through polarization by the substrate, in order to produce these superlattices. At low adatom density, higher adatom mobility allows the formation of incommensurate arrangements, while at higher adatom density, the repulsive force between adatoms could suppress adatom diffusion and form these stable commensurate arrangements. The differences in polarization of Sn adatoms in different orders were further confirmed by their apparent heights in STM images, measured over a wide bias range, as shown in Figure 3e-g. Under all the measured bias ranges, Sn adatoms in type A order show larger apparent height than in type B order, while Sn adatoms in type B orders exhibit a similar apparent height.

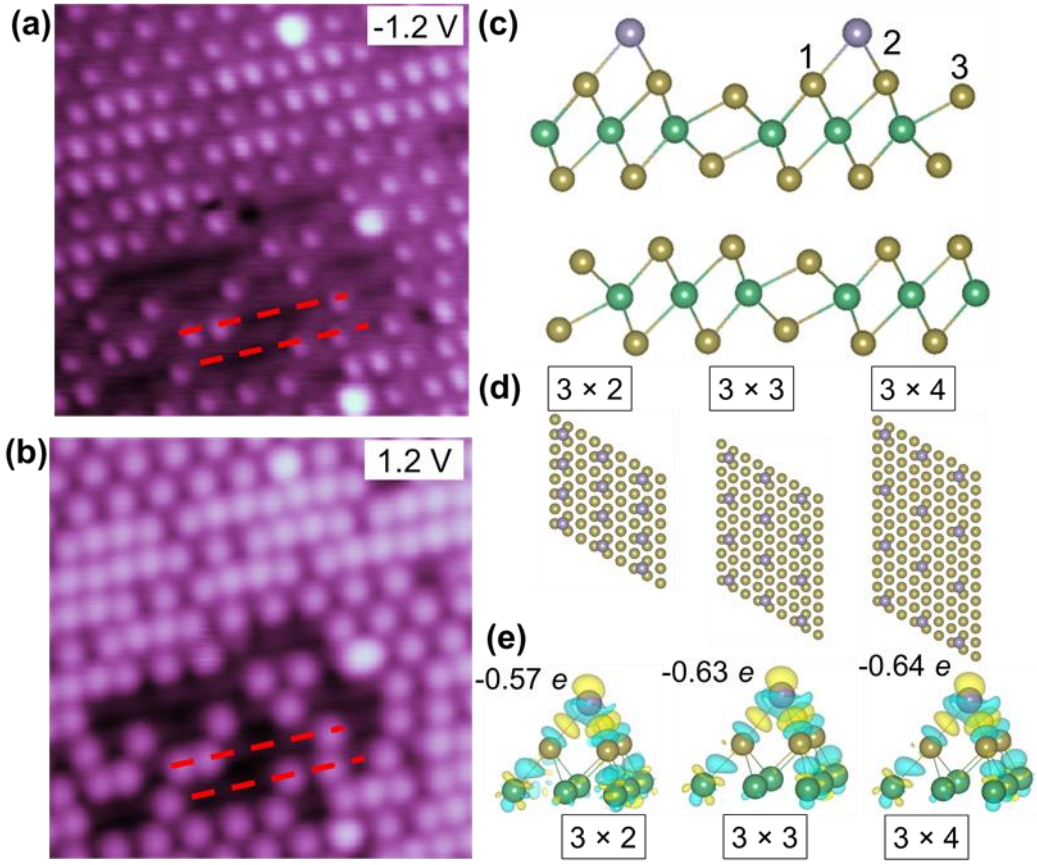

Figure 4. (a) and (b) STM images of the selected area with part of the Sn adatoms removed from the surface at different bias values of -1.2 V (a) and 1.2 V (b), respectively. (c) DFT calculations of the optimized location of Sn adatoms on the surface of $NbTe_2$. (d) The optimized configurations of Sn adatoms in 3 × 2, 3 × 3, and 3 × 4 superlattices. (e) The calculated amount of charge transfer between Sn adatoms and their corresponding differential charge density.

To further clarify the nature of the polarization induced by charge transfer, we have carried out DFT calculations on the configurations and charge transfer of the 3 × 2, 3 × 3, and 3 × 4 orders on the surface. The spatial location of Sn adatoms along the stripe direction was first determined by STM images, as shown in **Figure 4a** and 4b, in which part of the Sn adatoms were removed from the surface by scanning the selected area with an extremely low sample bias of -3 mV. As discussed in relation to Figure 2, the stripes induced by the 3 × 1 CDW turned out to be valleys on the surfaces due to the existence of a √19 × 3√3/2 CDW, which is marked by the red dashed lines in Figure 4a and 4b. The 1D Sn superlattices, therefore, can be determined to be very close to the top Te atoms along the stripes. Based on this result, the optimized configurations of the superlattices were obtained through calculations, with Sn adatoms located between the Te1 and Te2 atoms, as presented in Figure 4c. Top views of the optimized configurations of these three superlattices are shown in Figure 4d. Their calculated adsorption energies are -2.12 eV for 3 × 2, -2.19 eV for 3 × 3, and -2.25 eV for 3 × 4, suggesting that they are energy favorable. In addition, through calculations, it was determined that each Sn adatom in the 3 × 3 order and 3 × 4 order could donate 0.63 e and 0.64 e to the substrate, respectively, which are more than that of 0.57 e for the 3 × 2 order, as shown in Figure 4e. This coincides with the result that Sn adatoms in 3 × b (b = 3 to 8) orders have similar apparent heights in STM images, which are smaller than for the 3 × 2 order, because a larger amount of charge transfer could result in stronger bonding strength with the substrate and a shorter bonding length, and consequently, smaller apparent height in STM images. This result is also consistent with the calculated bond lengths, as summarized in Table S1 of the Supporting Information.

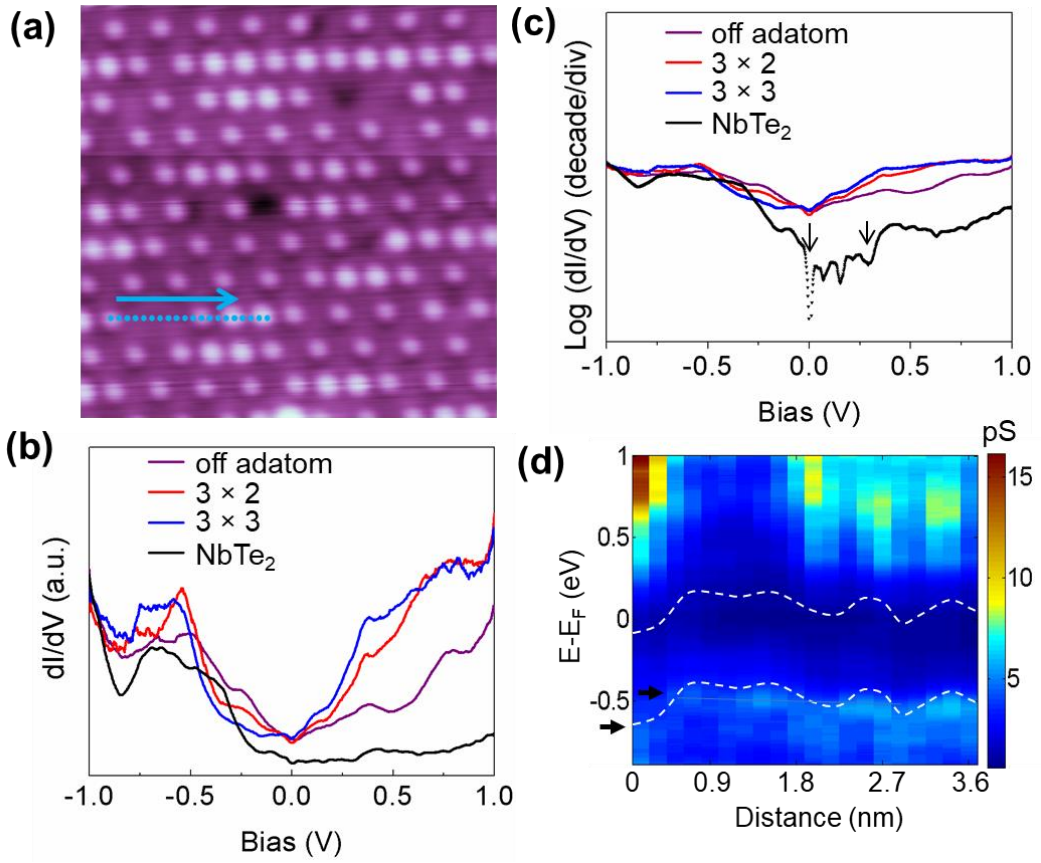

Figure 5. (a) STM image of an area with commensurate 1D Sn superlattices. (b) STS spectra of the $NbTe_2$ substrate, and on/off Sn adatoms in the 3 × 3 order and in the 3 × 2 order. (c) Logarithmic plots of the STS spectra in b to obtain the suppression of the local density of states (LDOS) near the Fermi level for the $NbTe_2$ substrate. (d) Spatially resolved *dI*/*dV* spectra along the dashed line in a, crossing Sn adatoms and the bare substrate.

The effects of Sn adatoms on the electronic properties of $NbTe_2$ substrate were further explored by STS measurements. As shown in the STS data in **Figure 5**, pure $NbTe_2$ substrate exhibited a semi-metallic characteristic with a pseudogap of around 0.3 eV (Figure 5b and 5c), as indicated by the black arrows. After deposition of Sn atoms, the STS spectra of both on and off Sn adatoms presented metallic characteristic, indicating the global effect of Sn superlattices on modifying the electronic properties of the substrate. Figure 5d shows spatially resolved *dI*/*dV* plots along one stripe and simultaneously across Sn adatoms and the bare substrate, which is marked in Figure 5a. It clearly shows a periodic distribution of the surface electronic states that matches the spatial position of Sn adatoms, as indicated by the white dashed lines. An apparent shift of ~ 0.16 eV was observed on the STS spectra of Sn adatoms in type B orders, compared with type A order and the bare substrate, as indicated by the two black arrows in Figure 5d.

This shift agrees with the result that Sn adatoms in type B donate more electrons to the substrate. These results verify the hypothesis that the surface electronic structure plays a decisive role in the adsorption scheme of the Sn adatoms. In addition, the periodic destruction of the surface electronic states of the Sn/$NbTe_2$ system also exhibits potential for modifying the active sites of heterogeneous catalysts through surface functionalization.

In summary, monatomic Sn superlattices were fabricated on the surface of $NbTe_2$, with a subtle balance between the CDW of the substrate and the indirect repulsive interaction between Sn adatoms. The well-dispersed monatomic characteristic of Sn adatoms not only demonstrates how the CDW can modulate the adsorption scheme of a reactant, but also demonstrates an effective means of utilizing CDW phase for fabricating heterogeneous ordered single-atom or nanocluster systems. The CDW in TMDs then is expected to be applied in both tuning the catalytic properties of TMD based materials and in epitaxial growth of other low-dimensional materials. This work could inspire the design and synthesis of new ordered superlattices on new TMD-based functional materials.

Experimental Section

Fresh $NbTe_2$ surface was obtained through in-situ cleaving by tapes in a load-lock chamber under vacuum of 1×10^{-8} Torr. Then, the sample was quickly transferred to ultra-high vacuum (UHV) conditions (better than 1×10^{-10} Torr). STM and STS characterization were performed in a low temperature STM (USM 1500-M, Unisoku Co.) at 78 K. During the STM and STS tests, voltage was applied to the sample. Sn adatoms on $NbTe_2$ substrate were fabricated by evaporation of Sn from a home-made crucible in a preparation chamber under UHV conditions and room temperature. The sample was then transferred to the STM chamber under UHV for further characterization. The *dI*/*dV* measurements were acquired with a lock-in technique with a sample voltage modulation of 10 mV at 937 Hz. The STM images were analyzed using WSxM software.[49]

All DFT calculations were performed using the Vienna Ab Initio Simulation Package (VASP).[50] The generalized gradient approximation (GGA) was applied to treat the exchange correlation energy with the Perdew-Burke-Ernzerhof (PBE) functional.[51] The projector augmented wave (PAW) method[52] was employed to describe electron-ion interactions with the cut-off energy of 500 eV. The structural models of $NbTe_2$ superstructures were constructed with two $NbTe_2$ layers. A vacuum spacing of 20 Å was built in to avoid interaction between adjacent surfaces. All structures in the calculations were relaxed until the convergence tolerance of force on each atom was smaller than 0.01 eV. The energy convergence criterion was set at 1×10^{-5} eV for self-consistent calculations.

The adsorption energy of Sn adatoms on the surface (E_{ad}) is calculated as

$$E_{ad} = (E_{total} - E_{substrate} - \mu_{Sn}) \quad \text{Equation (1)}$$

Here, E_{total} is the total energy of Sn on $NbTe_2$, $E_{substrate}$ is the total energy of $NbTe_2$, and μ_{Sn} is the chemical potential of a Sn atom, referring to the energy per atom in the elementary substance.

Supporting Information
Supporting Information is available from the Wiley Online Library or from the author.

Acknowledgements
This work is financially supported by Australian Research Council Discovery Projects and a Future Fellowship (DP160102627, DP170101467, and FT180100585) and by the Natural Science Foundation of China (11874003, 51672018, 51472016). The work was also partially supported by the Beijing Natural Science Foundation. Y. Liu acknowledge the support from the China Scholarship Council (CSC). The authors thank Dr. Tania Silver for critical reading of the manuscript.

Received: ((will be filled in by the editorial staff))
Revised: ((will be filled in by the editorial staff))
Published online: ((will be filled in by the editorial staff))

References

[1] H. Li, J. Wu, Z. Yin, H. Zhang, *Acc. Chem. Res.* **2014**, *47*, 1067.

[2] J. N. Coleman, M. Lotya, A. O'Neill, S. D. Bergin, P. J. King, U. Khan, K. Young, A. Gaucher, S. De, R. J. Smith, I. V. Shvets, S. K. Arora, G. Stanton, H.-Y. Kim, K. Lee, G. T. Kim, G. S. Duesberg, T. Hallam, J. J. Boland, J. J. Wang, J. F. Donegan, J. C. Grunlan, G. Moriarty, A. Shmeliov, R. J. Nicholls, J. M. Perkins, E. M. Grieveson, K. Theuwissen, D. W. McComb, P. D. Nellist, V. Nicolosi, *Science* **2011**, *331*, 568.

[3] K.-K. Liu, W. Zhang, Y.-H. Lee, Y.-C. Lin, M.-T. Chang, C.-Y. Su, C.-S. Chang, H. Li, Y. Shi, H. Zhang, C.-S. Lai, L.-J. Li, *Nano Lett.* **2012**, *12*, 1538.

[4] Y. Zhang, T.-R. Chang, B. Zhu, Y.-T. Cui, H. Yan, Z. Liu, F. Schmitt, J. Lee, R. Moore, Y. Chen, H. Lin, H.-T. Jeng, S.-K. Mo, Z. Hussain, A. Bansil, Z.-X. Shen, *Nat. Nanotech.* **2014**, *9*, 111.

[5] Q. H. Wang, K. Kalantar-Zadeh, A. Kis, J. N. Coleman, M. S. Strano, *Nat. Nanotech.* **2012**, *7*, 699.

[6] M. M. Ugeda, A. J. Bradley, Y. Zhang, S. Onishi, Y. Chen, W. Ruan, C. Ojeda-Aristizabal, H. Ryu, M. T. Edmonds, H.-Z. Tsai, A. Riss, S.-K. Mo, D. Lee, A. Zettl, Z. Hussain, Z. X. Shen, M. F. Crommie, *Nat. Phys.* **2016**, *21*, 92.

[7] K. Den, G. Wan, P. Deng, K. Zhang, S. Ding, E. Wang, M. Yan, H. Huang, H. Zhang, Z. Xu, J. Denlinger, A. Fedorov, H. Yang, W. Duan, H. Yao, Y. Wu, S. Fan, H. Zhang, X. Chen, S. Zhou, *Nat. Phys.* **2016**, *12*, 1105.

[8] J. A. Wilson, F. J. D. Salvo, S. Mahajan, *Adv. Phys.* **1975**, *24*, 117.

[9] D. Xiang, T. Liu, J. Xu, J. Y. Tan, Z. Hu, B. Lei, Y. Zheng, J. Wu, A. H. C. Neto, L. Liu, W. Chen, *Nat. Coummun.* **2018**, *9*, 2966.

[10] B. Lei, Y. Pan, Z. Hu, J. Zhang, D. Xiang, Y. Zheng, R. Guo, C. Han, L. Wang, J. Lu, L. Yang, W. Chen, *ACS Nano* **2018**, *12*, 2070.

[11] B. Lei, Z. Hu, D. Xiang, J. Wang, G. Eda, C. Han, W. Chen, *Nano Res.* **2017**, *10*, 1282.

[12] T. Straub, T. Finteis, R. Claessen, P. Steiner, S. Hüfner, P. Blaha, C. S. Oglesby, E. Bucher, *Phys. Rev. Lett.* **1999**, *82*, 4504.

[13] T. M. Rice, G. K. Scott, *Phys. Rev. Lett.* **1975**, *35*, 120.

[14] T. Kiss, T. Yokoya, A. Chainani, S. Shin, T. Hanaguri, M. Nohara, H. Takagi, *Nat. Phys.* **2007**, *3*, 720.

[15] F. Weber, S. Rosenkranz, J.-P. Castellan, R. Osborn, R. Hott, R. Heid, K.-P. Bohnen, T. Egami, A. H. Said, D. Reznik, *Phys. Rev. Lett.* **2011**, *107*, 107403.

[16] C. J. Arguello, E. P. Rosenthal, E. F. Andrade, W. Jin, P. C. Yeh, N. Zaki, S. Jia, R. J. Cava, R. M. Fernandes, A. J. Millis, T. Valla, R. M. Osgood, A. N. Pasupathy, *Phys. Rev. Lett.* **2015**, *114*, 037001.

[17] A. Soumyanarayanan, M. M. Yee, Y. He, J. van Wezel, D. J. Rahn, K. Rossnagel, E. W. Hudson, M. R. Norman, J. E. Hoffman, *Proc. Natl. Acad. Sci. USA* **2013**, *110*, 1623.

[18] H. Ryu, Y. Chen, H. Kim, H.-Z. Tsai, S. Tang, J. Jiang, F. Liou, S. Kahn, C. Jia, A. A. Omrani, J. H. Shim, Z. Hussain, Z.-X. Shen, K. Kim, B. Min, C. Hwang, M. F. Crommie, S.-K. Mo, *Nano Lett.* **2018**, *18*, 689.

[19] E. Morosan, H. W. Zandbergen, B. S. Dennis, J. W. G. Bos, Y. Onose, T. Klimczuk, A. P. Ramirez, N. P. Ong, R. J. Cava, *Nat. Phys.* **2006**, *2*, 544.

[20] S. A. Kivelson, E. Fradkin, V. J. Emery, *Nature* **1998**, *393*, 550.

[21] M. Eichberger, H. Schäfer, M. Krumova, M. Beyer, J. Demsar, H. Berger, G. Moriena, G. Sciaini, R. J. D. Miller, *Nature* **2010**, *468*, 799.

[22] L. J. Li, E. C. T. O'Farrell, K. P. Loh, G. Eda, B. Özyilmaz, A. H. C. Neto, *Nature* **2016**, *529*, 185.

[23] I. Vaskivskyi, I. A. Mihailovic, S. Brazovskii, J. Gospodaric, T. Mertelj, D. Svetin, P. Sutar, D. Mihailovic, *Nat. Commun.* **2016**, *7*, 11442.

[24] P. Chen, Y.-H. Chan, X.-Y. Fang, Y. Zhang, M. Y. Chou, S.-K. Mo, Z. Hussain, A.-V. Fedorov, T.-C. Chiang, T.-C. *Nat. Commun.* **2015**, *6*, 8943.

[25] M. Yoshida, R. Suzuki, Y. Zhang, M. Nakano, Y. Iwasa, *Sci. Adv.* **2015**, *1*, e1500606.

[26] I. Vaskivskyi, J. Gospodaric, S. Brazovskii, D. Svetin, P. Sutar, E. Goreshnik, I. A.

Mihailovic, T. Mertelj, D. Mihailovic, *Sci. Adv.* **2015**, *1*, e1500168.

[27] K. Sun, S. Sun, C. Zhu, H. Tian, H. Yang, J. Li, *Sci. Adv.* **2018**, *4*, eaas9660.

[28] Z. Zhang, J. Niu, P. Yang, Y. Gong, Q. Ji, J. Shi, Q. Fang, S. Jiang, H. Li, X. Zhou, L. Gu, X. Wu, Y. Zhang, *Adv. Mater.* **2017**, *29*, 1702359.

[29] J. Shi, X. Chen, L. Zhao, Y. Gong, M. Hong, Y. Huan, Z. Zhang, P. Yang, Y. Li, Q. Zhang, Q. Zhang, L. Gu, H. Chen, J. Wang, S. Deng, N. Xu, Y. Zhang, *Adv. Mater.* **2018**, *30*, 1804616.

[30] T. Liu, D. Xiang, Y. Zheng, Y. Wang, X. Wang, L. Wang, J. He, L. Liu, W. Chen, *Adv. Mater.* **2018**, *30*, 1804470.

[31] M. Chhowalla, H. K. Shin, G. Eda, L. J. Li, K. P. Loh, H. Zhang, *Nat. Chem.* **2013**, *5*, 263.

[32] J. Shi, X. Wang, S, Zhang, L. Xiao, Y. Huan, Y. Gong, Z. Zhang, Y. Li, X. Zhou, M. Hong, Q. Fang, Q. Zhang, X. Liu, L. Gu, Z. Liu, Y. Zhang, *Nat. Commun.* **2017**, *8*, 958.

[33] J. Feng, X. Sun, C. Wu, L. Peng, C. Lin, S. Hu, J. Yang, Y. Xie, *J. Am. Chem. Soc.* **2011**, *133*, 17832.

[34] V. R. Stamenkovic, B. Fowler, B. S. Mun, G. Wang, P. N. Ross, C. A. Lucas, N. M. Marković, *Science* **2007**, *315*, 493.

[35] F. Zaera, *Prog. Surf. Sci.* **2001**, *69*, 1.

[36] G. Chen, C. Xu, X. Huang, J. Ye, L. Gu, G. Li, Z. Tang, B. Wu, H. Yang, Z. Zhao, Z. Zhou, G. Fu, N. Zheng, *Nat. Mater.* **2016**, *15*, 564.

[37] Q. Feng, S. Zhao, Y. Wang, J. Dong, W. Chen, D. He, D. Wang, J. Yang, Y. Zhu, H. Zhu, L. Gu, Z. Li, Y. Liu, R. Yu, J. Li, Y. Li, *J. Am. Chem. Soc.* **2017**, *139*, 7294.

[38] C. Battaglia, H. Cercellier, F. Clerc, L. Despont, M. G. Garnier, C. Koitzsch, P. Aebi, *Phys. Rev. B* **2005**, *72*, 195114.

[39] J. A. Wilson, *Phys. Rev. B* **1978**, *17*, 3880.

[40] S. T. Marshall, M. O'Brien, B. Oetter, A. Corpuz, R. M. Richards, D. K. Schwartz, J. W.

Medlin, *Nat. Mater.* **2010**, *9*, 853.

[41] J. Balajka, M. A. Hines, W. J. I. DeBenedetti, M. Komora, J. Pavelec, M. Schmid, U. Diebold, *Science* **2018**, *361*, 786.

[42] H. Brune, M. Giovannini, K. Bromann, K. Kern, *Nature* **1988**, *394*, 451.

[43] F. E. Kalff, M. P. Rebergen, E. Fahrenfort, J. Girovsky, R. Toskovic, J. L. Lado, J. Fernández-Rossier, A. F. Otte, *Nat. Nanotech.* **2016**, *11*, 926.

[44] D. Cukjati, A. Prodan, N. Jug, H. J. P. van Midden, P. Starowicz, E. Karič, S. W. Hla, H. Böhm, F. W. Boswell, J. C. Bennett, *J. Cryst. Growth* **2002**, *237–239*, 278.

[45] J. van Landuyt, G. van Tendeloo, S. Amelinckx, *Phys. Status Solidi A* **1974**, *26*, 585.

[46] S. Zhang, P. Kang, T. J. Meyer, *J. Am. Chem. Soc.* **2014**, *136*, 1734.

[47] Y. Chen, M. W. Kanan, *J. Am. Chem. Soc.* **2012**, *134*, 1986.

[48] S. J. Freakley, Q. He, J. H. Harrhy, L. Lu, D. A. Crole, D. J. Morgan, E. N. Ntainjua, J. K. Edwards, A. F. Carley, A. Y. Borisevich, C. J. Kiely, G. J. Hutchings, *Science* **2016**, *351*, 965.

[49] I. Horcas, R. Fernández, J. M. Gómez-Rodríguez, J. Colchero, J. Gómez-Herrero, A. M. Baro, *Rev. Sci. Instrum.* **2007**, *78*, 013705.

[50] J. Hafner, *J. Comput. Chem.* **2008**, *29*, 2045.

[51] J. P. Perdew, K. Burke, M. Ernzerhof, *Phys. Rev. Lett.* **1996**, *77*, 3865.

[52] P. E. Blochl, *Phys. Rev. B* **1994**, *50*, 17953.

TOC

Applying the CDW of $NbTe_2$ to generate the assembling adsorption of Sn adatoms on the surface. The CDW modulated superlattices could in turn change the surface electronic properties from semi-metallic to metallic. These results demonstrate an effective approach in tuning the surface chemical properties of TMD based materials by theirs CDWs.